analytical chemistry

pubs.acs.org/ac Article

Efficient DNA Walker Guided with Well-Regulated Interfacial Tracks for Ultrasensitive Electrochemiluminescence Biosensing

Heye Lv,[⊥] Anyi Chen,[⊥] Wenqian Cheng, Liangsheng Kong, Min Zhao,* Shijia Ding, Huangxian Ju, and Wei Cheng*

Cite This: *Anal. Chem.* 2020, 92, 15624−15631 Read Online

ACCESS | Metrics & More | Article Recommendations | Supporting Information

ABSTRACT: Herein, highly efficient deoxyribonucleic acid (DNA) walking on electrode surfaces was realized by regulating DNA tracks, which was applied to construct an ultrasensitive electrochemiluminescent (ECL) biosensor for BCR/ABL fusion gene detection. The well-regulated DNA tracks were constructed *via* supersandwich hybridization chain reaction of two DNA strands (L_1 and L_2) to generate periodic linear dsDNA concatemers, where an exposed L_1 domain closed with blocking strands (BS). The prepared DNA tracks were further assembled onto the surface of the Au nanoparticle-functionalized g-C_3N_4 nanohybrid (Au@g-C_3N_4 NHs)-modified electrode, achieving well-regulated interfacial tracks for the DNA walker. On this state, folic acid-labeled BS (FA-BS) were close to Au@g-C_3N_4 NHs, performing a quenched ECL emission. With existence of the BCR/ABL fusion gene, the target combined two walking DNA strands (WD_1 and WD_2) to form the bipedal DNA walkers, which walked on the well-regulated interfacial DNA tracks and replaced the FA-BS to light up the ECL emission, realizing DNA walker-based signal amplification. Compared to randomly constructed DNA tracks, the well-regulated DNA tracks reduced the kinetics barrier and fitted the step size of the DNA walker, thus promoting the DNA walking efficiency and decreasing the risk of interruption in the walking process. As a result, the designed DNA walker presented higher efficiency and capacity in signal amplification. Benefiting from this efficient DNA walker strategy, the ECL biosensor achieved sensitive detection of the BCR/ABL fusion gene with a detection limit of 0.18 fM. This smart strategy proposed a brief strategy to promote the working efficiency of the biosensor, which presented great application potential in clinical molecular diagnosis.

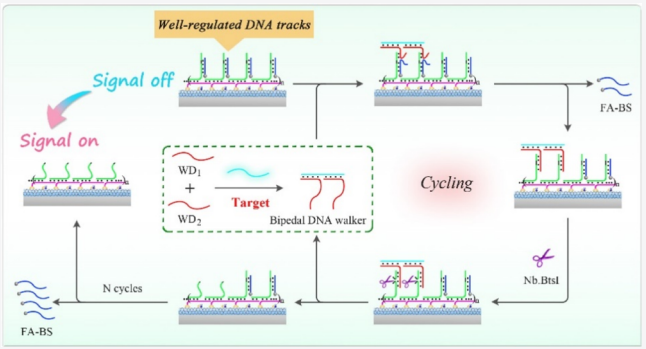

INTRODUCTION

Inspired by the biological protein motors, deoxyribonucleic acid (DNA) walkers have been constructed to move progressively and autonomously along predetermined tracks by biasing Brownian motion with chemical energy.[1−3] Structurally, DNA walkers operate as a three-component system: (i) fuel molecules or other forms of energy input driving the motion, (ii) walkers consisting of legs or feet, (iii) tracks overhanging single-stranded branches as footholds.[4] DNA walkers have been developed and applied in the field of biosensing,[5−7] biological imaging,[8−10] and cargo delivery[11] for the transduction and amplification of signals. Especially, DNA walkers present outstanding advantages in the construction of biosensors,[12,13] which is attributable that DNA walking reactions are much more efficient than traditional interface reactions because of the increased local concentration of DNA strands.[14,15] However, restricted by the inefficient interface reactions, current biosensors commonly still present longer responsive time than homogeneous assays despite the acceleration by DNA walker.[16−18] Moreover, the moving of DNA walker is concerned with the size, which brings about the risk of interruption and limits the maximum steps. Therefore, it is strongly demanded to design DNA walkers with higher moving efficiency and more walking steps, which would facilitate biosensors with excellent responsive speed and signal amplification capacity.

DNA tracks are the key component that guide the movement of DNA walkers.[19−21] During the DNA walking process, the movement range and processivity efficiency of DNA walkers rely on the dynamic interactions between the walking strand and the prescribed tracks. Therefore, the smart design and assembly quality of certain tracks are a decisive factor that determines the walking efficiency of the DNA

Received: September 14, 2020
Accepted: October 28, 2020
Published: November 10, 2020

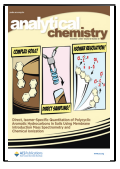

https://dx.doi.org/10.1021/acs.analchem.0c03893
Anal. Chem. 2020, 92, 15624−15631

Scheme 1. Schematic Diagrams of the Ultrasensitive "Off-On" ECL Biosensing for BCR/ABL Fusion Gene Determination on Basis of the Well-Regulated Track-Based DNA Walker and Au@g-C_3N_4 NHs[a]

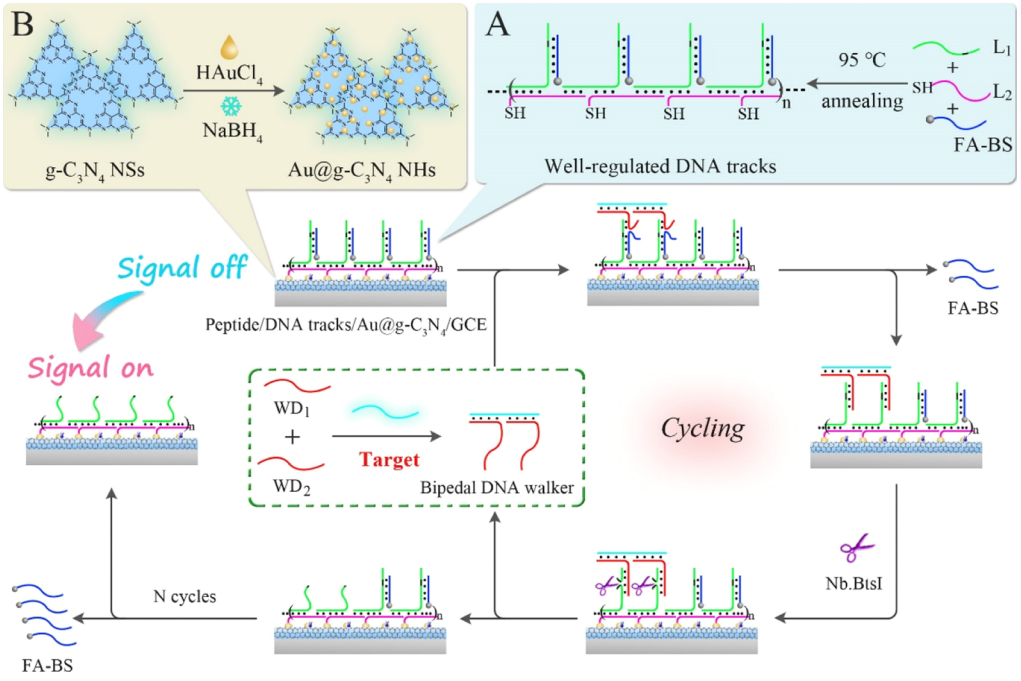

[a]The preparation of the (A) well-regulated DNA tracks and the (B) Au@g-C_3N_4 NHs.

walkers. At present, most well-defined DNA tracks are constructed by randomly fabricating DNA molecules onto the interface, which brings about the disordered arrangement of tracks, thus limiting the moving efficiency of the DNA walker.[22−24] On the one hand, the tangle of DNA strands increases the barrier of DNA reaction, thus decreasing the reaction rate. On the other hand, the walking could be interrupted by the excessive interval of partial DNA tracks. In this perspective, well-regulated DNA tracks are expected to promote the moving rate and efficiency of DNA walkers, thereby increasing signal response rate as well as amplification capability in bioanalysis applications.

Here, long periodic linear DNA concatemers were assembled onto the interface to engineer well-regulated DNA tracks, which could effectively improve the movement efficiency of DNA walkers on the electrode surface. As a proof of concept, well-regulated interfacial track-based bipedal DNA walker was designed for the first time, which further combined with a Au nanoparticle (Au NP)-functionalized g-C_3N_4 nanohybrid (Au@g-C_3-N_4)-based electrochemiluminescence (ECL) system to develop ultrasensitive ECL biosensing for BCR/ABL fusion gene determination. The principle of programmed DNA tracks is exhibited in Scheme 1A. Two ssDNAs (L_1 and L_2) were hybridized *via* the supersandwich hybridization chain reaction to form the periodic linear dsDNA concatemers, where the exposed L_1 domain acts as the equidistant foothold. The foothold was further blocked by the BS strand to form the well-regulated DNA tracks *via* one-step approach. Moreover, Au@g-C_3N_4 NHs prepared by *in situ* reduction of Au NPs with sodium borohydride ($NaBH_4$) onto the g-C_3N_4 NSs (Scheme 1B) were used to modify the electrode interface for providing numerous active sites. Next, the pre-assembled tracks were immobilized onto the Au@g-C_3N_4 NHs modified electrode *via* the Au−S bond. Because of BS of tracks labeled with folic acid (FA), the ECL signal of Au@g-C_3N_4/$S_2O_8^{2-}$ system was quenched by FA to obtain a "signal-off" state. In the presence of the target BCR/ABL fusion gene, a pair of walking DNA strands (WD_1, WD_2) was designed to specifically recognize the target BCR/ABL fusion gene for the bipedal DNA walker formation. The formed bipedal DNA walker could displace the prehybridized FA-BS from the interfacial tracks by proximity binding-induced DNA strand displacement reaction. Fueled by nicking endonuclease (Nb.BtsI), bipedal DNA walker was able to move along the tracks by cleaving the foothold of the tracks at every step with the release of the bipedal DNA walker. With the help of autonomous and multiple-step walking behaviors like this, vast majority of FA-BS was removed from the modified electrode interface, realizing the ECL signal recovery ("signal-on" state) for highly sensitive target BCR/ABL fusion gene detection. Significantly, equidistant footholds are designed in the programmed interfacial track, of which the invariable distance is well matched to the bipedal DNA walker. Compared with stochastic tracks, this design allows the bipedal DNA walkers to move along well-regulated tracks with higher movement efficiency to achieve rapid and sensitive signal amplification. This well-regulated track-based DNA walker provides a new idea for movement efficiency improvement in DNA walking nanomachine, exhibiting a huge potential in bioanalysis for signal amplification.

EXPERIMENTAL SECTION

Assembly of the Well-Regulated DNA Tracks. The mixture of the L_1 (1.0 μM), L_2 (1.0 μM), and FA-BS (1.0 μM) in DNA hybridization buffer was heated about 5 min at 95 °C and subsequently cooled down to room temperature for the DNA track (L_1/L_2/FA-BS) formation.

Polyacrylamide Gel Electrophoresis. To verify the successful assembly of the DNA tracks by L_1, L_2, and BS, polyacrylamide gel electrophoresis (PAGE) was performed.

https://dx.doi.org/10.1021/acs.analchem.0c03893
Anal. Chem. 2020, 92, 15624−15631

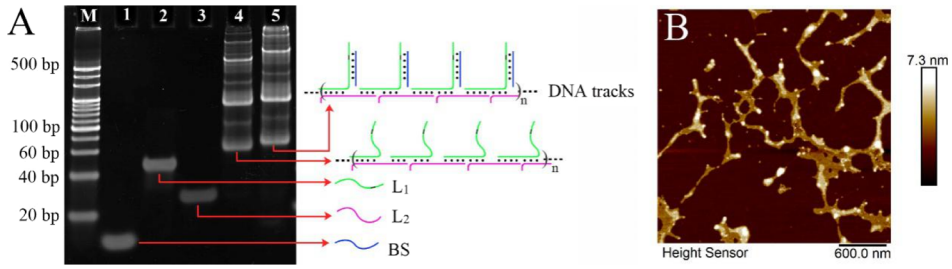

Figure 1. (A) PAGE analysis of DNA tracks. Lane 1: BS, lane 2: L_1, lane 3: L_2, lane 4: L_1 + L_2, lane 5: L_1 + L_2 + BS. (B) AFM image of three strands of L1, L2, and BS-generated long dsDNA concatemers. The concentrations of all sequences were 1 μM.

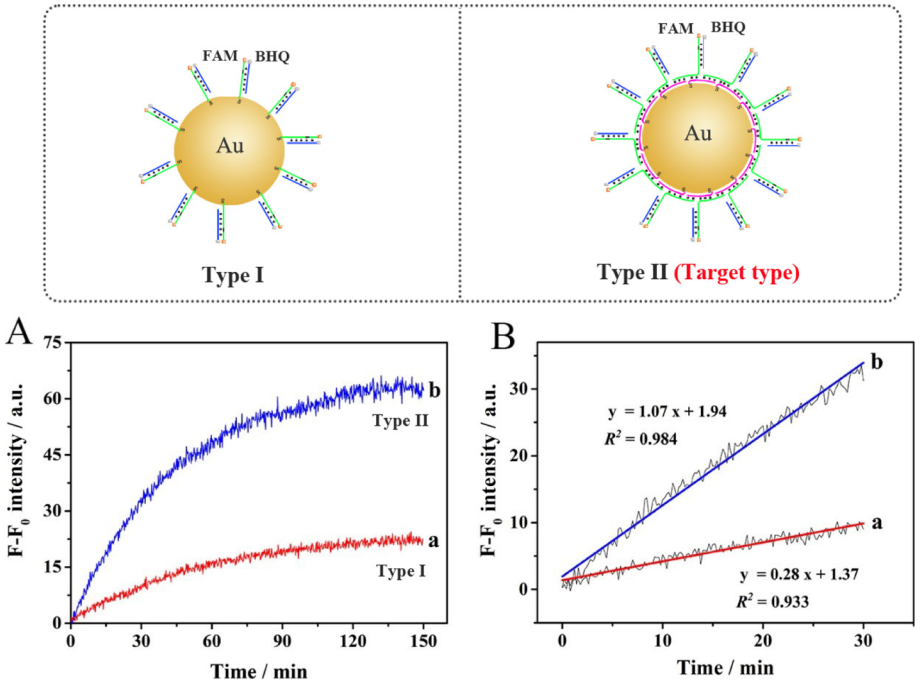

Figure 2. (A) Real-time fluorescence comparison between type I (a) and type II (b). (B) Comparison of initial walking rate between type I (a) and type II (b). The fluorescence signals were measured at fixed wavelength of 520 nm. F and F_0 were fluorescence signals related to control systems with or without the 100 pM target.

The samples were loaded into the premade native polyacrylamide gel (10%), and electrophoresis was carried out in 1×TBE buffer at 110 V for 35 min. After dying with GelRed, the gel was visualized using a gel image system.

Fabrication of Au@g-C_3N_4 NHs. The Au NP-functionalized g-C_3N_4 nanohybrids (Au@g-C_3N_4 NHs) were fabricated with a slight modification according to the literature.[25] First, 5 mg g-C_3N_4 NSs powder was dissolved in 5 mL of deionized water. Afterward, 70 μL of $HAuCl_4$ solution (1%) was injected to the prepared g-C_3N_4 NSs suspension. This above mixture was ultrasonically treated for 30 min and then stirred at room temperature for 1.5 h. The operation was repeated 3 times. Next, 125 μL of 10 mM freshly prepared $NaBH_4$ was rapidly dropped into the mixture to reduce $AuCl_4^-$. After constantly stirring for 20 min, 50 μL of 10 mM sodium citrate solution was injected slowly to the above mixture with stirring for 30 min. After that, the Au@g-C_3N_4 NHs were separated by centrifugation at 9000 rpm for 10 min and washed thoroughly with distilled water. Eventually, the precipitate was redispersed into 2 mL of deionized water for further use.

Construction of ECL Biosensor. First, the glassy carbon electrode (GCE, 3 mm in diameter) was polished by alumina slurry and next ultrasonicated in ultrapure water to obtain a cleaned electrode. Subsequently, 10 μL of fabricated Au@g-C_3N_4 NHs was assembled onto the cleaned GCE surface and dried at 37 °C to obtain a uniform film. Afterward, 10 μL of DNA tracks was incubated with the Au@g-C_3N_4 NH-coated electrode at 4 °C overnight. After being thoroughly rinsed with phosphate-buffered saline (PBS), the above-prepared electrode was further reacted with 10 μL of zwitterionic peptide (1 mg/mL) for 1 h to block nonspecific binding sites. Ultimately, the designed ECL biosensor was stored at 4 °C before use.

ECL Measurement Procedure. Prior to measurement, 10 μL of the walking DNA mixture (WD_1, WD_2, 1 nM), Nb.BtsI (0.1 U/μL) and various target concentrations in 1×CutSmart buffer was dropped on the constructed biosensing surface and then incubated at 37 °C for 1 h. Subsequently, the as-prepared electrode was rinsed with PBS buffer and conducted in 7 mM $K_2S_2O_8$ solution on the MPI-E multifunctional analyzer with a continuous potential scanning from −1.6 to 0 V at a scanning rate of 0.3 V/s (the voltage of the photomultiplier tube at 800 V).

https://dx.doi.org/10.1021/acs.analchem.0c03893
Anal. Chem. 2020, 92, 15624−15631

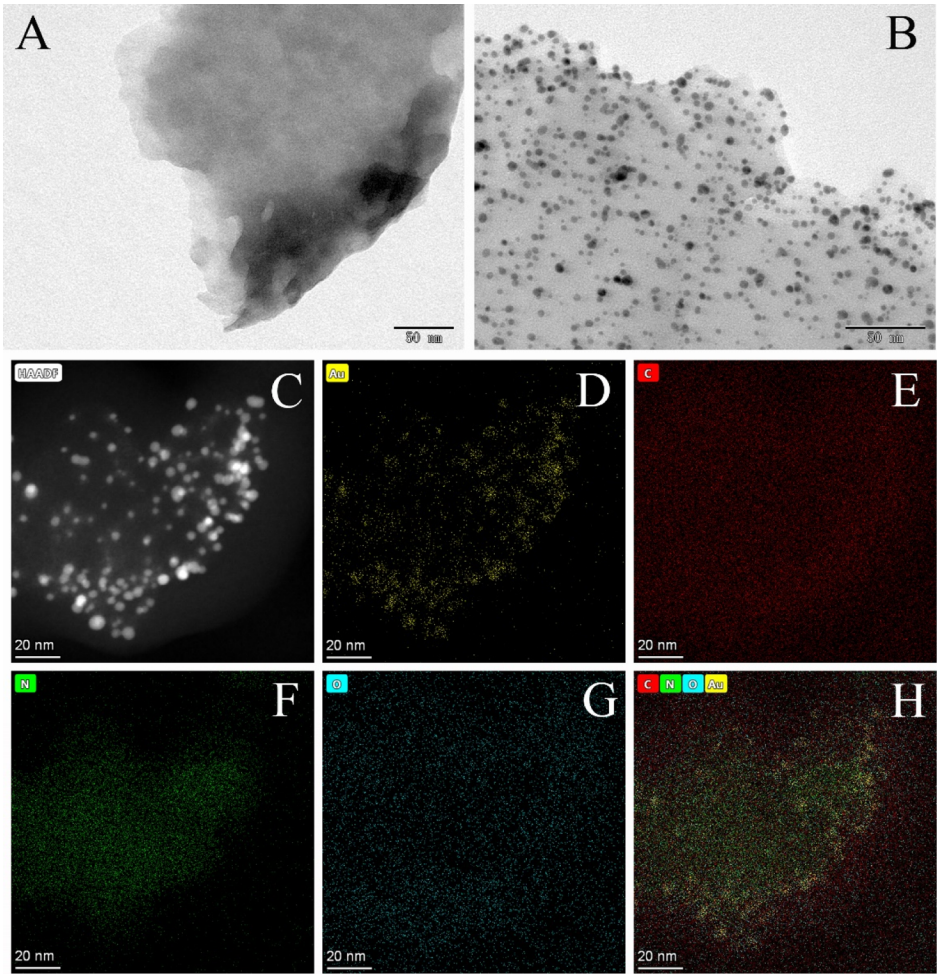

Figure 3. TEM images of (A) g-C_3N_4 NSs and (B) Au@g-C_3N_4 NHs. The HAADF-STEM image of Au@g-C_3N_4 NHs (C) and EDX elemental mappings of Au (D), C (E), N (F), and O (G).

RESULTS AND DISCUSSION

Characterization of DNA Tracks. The fabrication of DNA tracks had been evaluated by PAGE in Figure 1A. It could be seen that BS, L_1, and L_2 monomer in lane 1−3 represented distinct bands, respectively. Lane 4 exhibited ladder bands for the cross-hybridization of L_1 and L_2, which indicated the formation of long dsDNA concatemers. When BS were added into the mixture of L_1 and L_2, lower migration products were observed in lane 5, suggesting that BS were hybridized with the terminuses of L_1 and L_2 products to obtain DNA tracks. In addition, atomic force microscopy (AFM) was utilized to view the morphology of the three strands of L_1, L_2, and BS-generated long dsDNA concatemers. As expected, the submicrometer-long dsDNA nanowires (Figure 1B) were observed, showing a high yield and excellent homogeneity of DNA tracks.

Kinetics Study of Well-Regulated Interfacial Track-Based DNA Walker Amplification. To confirm the superiority of the well-regulated tracks in the DNA walker design, kinetic study of the bipedal DNA walker for walking efficiency was compared with the conventional DNA walker (stochastic assembly of DNA tracks). The comparative experiment was established by fabricating the different tracks on Au NPs: (a) stochastic track-based bipedal DNA walker as type I and (b) well-regulated track-based bipedal DNA walker as type II. Figure 2A demonstrated the real-time fluorescence curves of the bipedal DNA walkers in response to BCR/ABL fusion gene with the above two types. It could be seen that the type II (curve b) yielded a significantly increased $F - F_0$ signal, exhibiting a higher signal amplification and walking efficiency compared to the traditional type I (curve a). Furthermore, as shown in Figure 2B, according to the comparison of the initial rate between type I (curve a) and type II (curve b), the kinetics of type II had a 3.8-fold enhancement compared to that of the type I. These results indicated that the strategy of well-regulated DNA tracks enabled the walking of DNA walker with a faster kinetics to achieve efficient signal amplification in bioanalysis.

Characterization of Au@g-C_3N_4 NHs and g-C_3N_4 NSs. The transmission electron microscopy (TEM) was employed to monitor the morphologies of Au@g-C_3N_4 and g-C_3N_4 NSs. Figure 3A illustrates that the exfoliated g-C_3N_4 NSs presented a layered 2D structure.[26,27] After *in situ* reduction of Au NPs, massive Au NPs with a diameter of 5 nm were uniformly distributed on the surface of g-C_3N_4 NSs (Figure 3B), which revealed that Au NPs were tightly anchored on g-C_3N_4 NSs.

Further insights into the element distribution of Au@g-C_3N_4 NHs was verified by high-angle annular dark-field (HAADF)-scanning transmission electron microscopy (STEM) (Figure 3C) and energy-dispersive X-ray spectroscopy (EDX) elemental mapping. As expected, Au NPs with the main element of Au (yellow region, Figure 3D) were consistently

https://dx.doi.org/10.1021/acs.analchem.0c03893
Anal. Chem. 2020, 92, 15624−15631

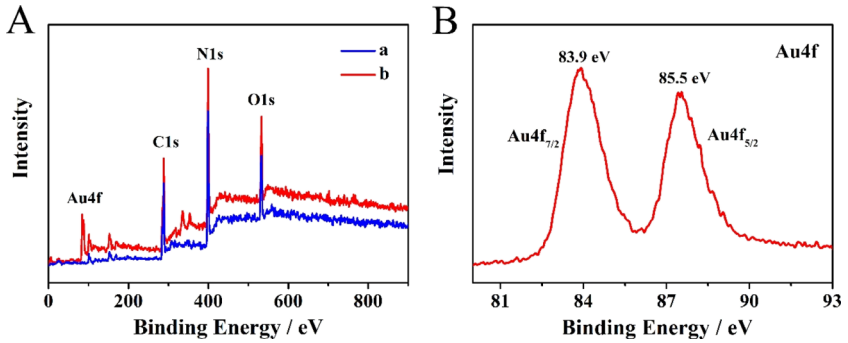

Figure 4. (A) XPS survey spectra of g-C_3N_4 NSs (a) and Au@g-C_3N_4 NHs (b). (B) High-resolution XPS spectrum of the Au 4f pattern from Au@g-C_3N_4 NHs.

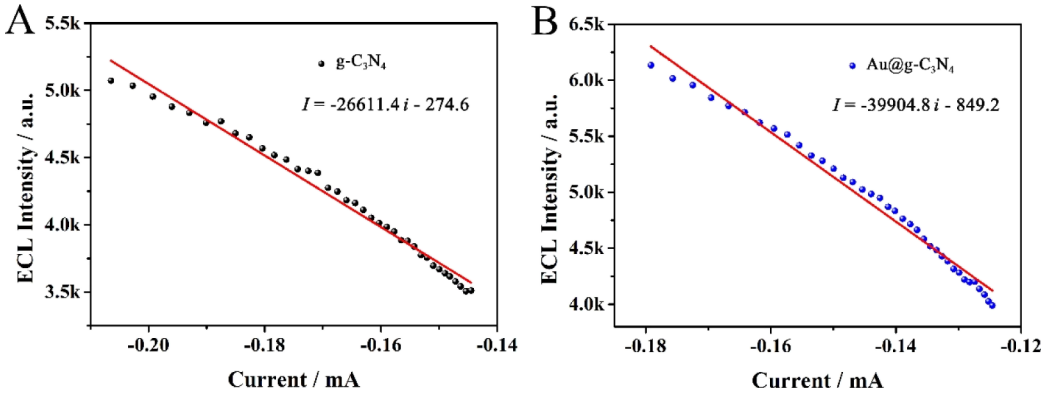

Figure 5. Calibration curve for the relationship between the ECL intensities and the currents of (A) g-C_3N_4 and (B) Au@g-C_3N_4.

distributed on the g-C_3N_4 NSs with main elements of C (red region, Figure 3E), N (green region, Figure 3F), and O (blue region, Figure 3G). It is worth mentioning that O element was ascribed to the adsorption of oxygen on g-C_3N_4 NSs during the polymerization process. It confirmed that Au NPs were decorated onto the surface of g-C_3N_4 NSs.

Moreover, the X-ray photoelectron spectrum (XPS) was also applied to verify the chemical composition of Au@g-C_3N_4 NHs. As shown in Figure 4A, the overall XPS spectra suggested C, N, O, and Au elements existed in Au@g-C_3N_4 NHs as dominant elemental components. The characteristic peaks of C 1s, N 1s, and O 1s were at 288.2, 398.7, and 549.0 eV, which originated from g-C_3N_4 NSs. The high-resolution XPS spectrum of the Au 4f pattern showed two peaks at 83.9 eV for Au $4f_{7/2}$ and 85.5 eV for Au $4f_{5/2}$ with a peak-to-peak distance of 1.6 eV (Figure 4B), indicating that the Au NPs were introduced into g-C_3N_4 NSs.

ECL Quantum Efficiency of Au@g-C_3N_4 NHs. The ECL quantum efficiency is an important parameter to evaluate the ECL performance of the luminophors. In order to confirm the ECL enhancement of Au NPs toward the g-C_3N_4, the relative ECL quantum efficiencies of Au@g-C_3N_4 to g-C_3N_4 are calculated by studying the linear relationship between the ECL signal and the currents of g-C_3N_4 (Figure 5A) and Au@g-C_3N_4 (Figure 5B), respectively. The experimental results indicated that the ECL intensity was proportional to the Faradaic current in the particular ECL system. According to the equation[28]

$$\phi_x = \phi_{st}\left(\frac{\int_0^t I\,dt}{\int_0^t i\,dt}\right)_x \Big/ \left(\frac{\int_0^t I\,dt}{\int_0^t i\,dt}\right)_{st} \quad (1)$$

The quantitative relations of between ECL intensity and current in g-C_3N_4 and Au@g-C_3N_4 system were defined as the following equations

$$I_{g\text{-}C_3N_4} = k_{g\text{-}C_3N_4} i_F = k_{g\text{-}C_3N_4}(i - i_n) = -26611.4i - 274.6 \quad (2)$$

$$I_{Au@g\text{-}C_3N_4} = k_{Au@g\text{-}C_3N_4} i_F = k_{Au@g\text{-}C_3N_4}(i - i_n) = -39904.8i - 849.2 \quad (3)$$

where the I, k, i_F, i_n, and t represented the ECL intensity, the slope of the linear response curve, Faradaic current, non-Faradic current, and time. Therefore, the quotient (Q) of $\phi_{g\text{-}C_3N_4}$ and $\phi_{Au@g\text{-}C_3N_4}$ could be calculated according to the following equation

$$Q = \frac{\phi_{Au@g\text{-}C_3N_4}}{\phi_{g\text{-}C_3N_4}} = \left(\frac{\int_0^t I\,dt}{\int_0^t i_F\,dt}\right)_{Au@g\text{-}C_3N_4} \Big/ \left(\frac{\int_0^t I\,dt}{\int_0^t i_F\,dt}\right)_{g\text{-}C_3N_4} = \left(\frac{\int_0^t k i_F\,dt}{\int_0^t i_F\,dt}\right)_{Au@g\text{-}C_3N_4} \Big/ \left(\frac{\int_0^t k i_F\,dt}{\int_0^t i_F\,dt}\right)_{g\text{-}C_3N_4} = \frac{k_{Au@g\text{-}C_3N_4}}{k_{g\text{-}C_3N_4}} = \frac{-39904.8}{-26611.4} = 1.5 \quad (4)$$

It could be seen that the ECL quantum efficiency of Au@g-C_3N_4 showed 1.5-fold enhancement than that of g-C_3N_4, which could be attributed to the higher electron transfer efficiency in the ECL process of Au@g-C_3N_4.

https://dx.doi.org/10.1021/acs.analchem.0c03893
Anal. Chem. 2020, 92, 15624−15631

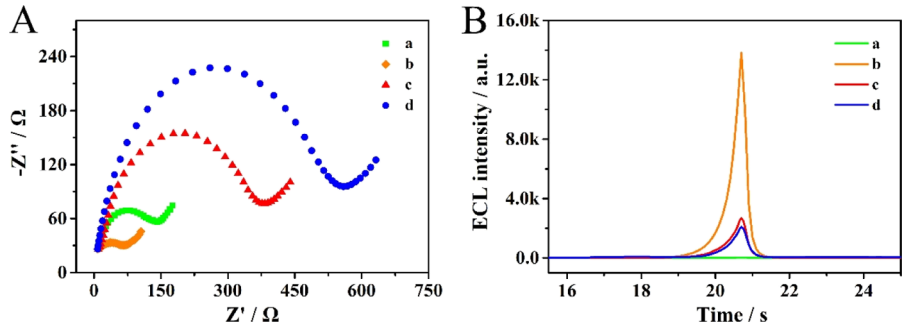

Figure 6. (A) EIS and (B) ECL time profiles of (a) bare GCE, (b) Au@g-C_3N_4/GCE, (c) DNA tracks/Au@g-C_3N_4/GCE, and (d) peptide/DNA tracks/Au@g-C_3N_4/GCE. The EIS measurement was carried out in the frequency range of 0.1 to 10^4 Hz with 5 mV amplitude. The ECL responses were obtained with a potential from −1.6 to 0 V at a scan rate of 0.3 V/s in 3 mL of 7 mM $K_2S_2O_8$.

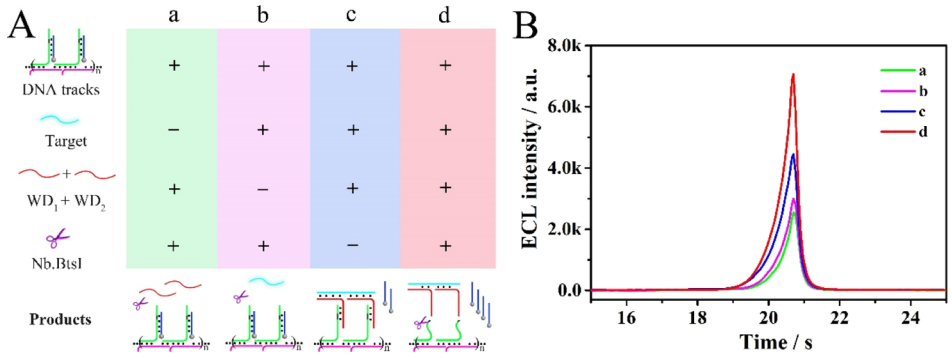

Figure 7. (A) Schematic illustration of control experiments. (B) Corresponding ECL signal of the modified electrodes (peptide/DNA tracks/Au@g-C_3N_4/GCE) incubated with the products of control experiments: (a) WD_1 + WD_2 + Nb.BtsI, (b) target + Nb.BtsI, (c) target + WD_1 + WD_2, and (d) target + WD_1 + WD_2 + Nb.BtsI. The concentration of target was 100 fM.

EIS and ECL Characterization of the Biosensor. The stepwise assembly of the biosensor was characterized by EIS measurements, which was performed in 5 mM $[Fe(CN)_6]^{3-/4-}$ containing 0.1 M KCl (Figure 6A). The semicircle diameter was equal to the electron transfer resistance (R_{et}). It could be clearly observed that the bare GCE showed a small semicircle because of a free electron-transfer process (curve a). When Au@g-C_3N_4 NHs were coated onto the GCE, one smaller semicircle domain was observed (curve b), revealing that Au@g-C_3N_4 NHs with excellent conductivity could accelerate electron transfer. A large semicircle domain was obtained when DNA tracks were modified on the Au@g-C_3N_4 NHs *via* Au−S bond (curve c), which was attributable that the negative charge of DNA tracks and their phosphate backbones prevented the electron transfer between electrode and $[Fe(CN)_6]^{3-/4-}$. After incubation with the zwitterionic peptide sealant, a larger R_{et} was observed because of the poor conductivity of the zwitterionic peptide (curve d).

To further confirm successful construction of the biosensor, the ECL intensities of distinctly modified electrodes were carried out in 7 mM $K_2S_2O_8$ (Figure 6B). With a bare GCE (curve a), no obvious ECL response was observed because of the absence of luminophores. When the electrode was immobilized with Au@g-C_3N_4 NHs, a strong ECL response was obtained (curve b), because Au@g-C_3N_4 NHs possessed excellent ECL performance. The ECL signal significantly declined when the modified electrode further assembled with DNA tracks (curve c), indicating that FA-BS from DNA tracks could vastly quench the ECL emission of the Au@g-C_3N_4 NHs/$K_2S_2O_8$ system. After the zwitterionic peptide was employed to block the nonspecific sites, the ECL signal decreased. These results verified that the stepwise assembly of the designed biosensor was successfully implemented, as expected.

Feasibility Study for BCR/ABL Fusion Gene Determination. To estimate the feasibility of the constructed biosensor for BCR/ABL fusion gene analysis on the basis of the well-regulated DNA walker for signal amplification, plenty of control experiments were implemented by the modified electrodes (peptide/DNA tracks/Au@g-C_3N_4/GCE) incubating with different products. As shown in Figure 7, the DNA walker was studied by selecting target (BCR/ABL fusion gene, 100 fM), WD_1, WD_2, and Nb.BtsI as the control conditions. When the mixture of WD_1, WD_2 and Nb.BtsI was added to the modified electrode, the ECL signal was about 2791 a.u. (curve a). Similarly, when the mixture of target and Nb.BtsI was dropped onto the electrode, a weak ECL intensity about 2996 a.u. (curve b) was observed. However, when the mixture of WD_1, WD_2, and target was dropped onto the electrode, the ECL signal increased to 4450 a.u. (curve c). The augment meant that bipedal DNA walker formed and replaced the prehybridized FA-BS from DNA tracks through target-induced proximity hybridization. Finally, when incubating the mixture of WD_1, WD_2, Nb.BtsI, and target with the electrode, a further raised ECL response about 7071 a.u.(curve d) was observed, illustrating that Nb.BtsI could induce the circle of target to release more FA-BS. These evidence manifested that the DNA walker mediated the isothermal signal amplification strategy could dramatically magnify the target-relevant signal for BCR/ABL fusion gene determination.

Performance of BCR/ABL Fusion Gene Assay. Various concentrations of BCR/ABL fusion gene were quantitatively

https://dx.doi.org/10.1021/acs.analchem.0c03893
Anal. Chem. 2020, 92, 15624−15631

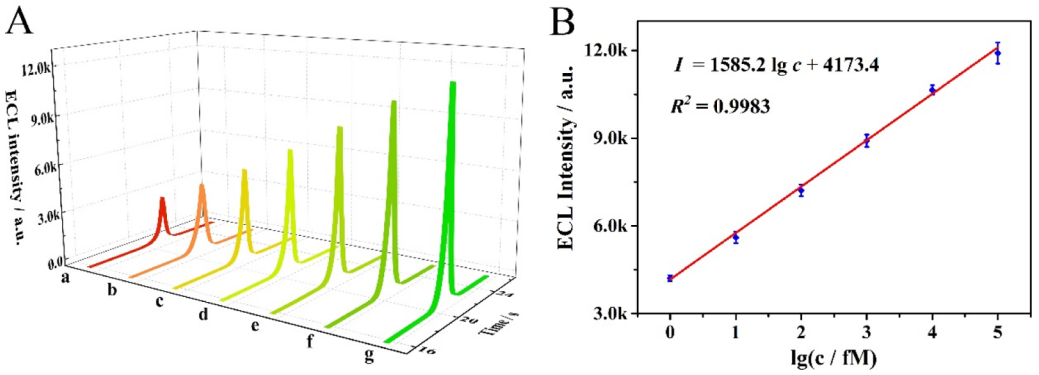

Figure 8. (A) ECL intensities of the biosensor incubated with various concentrations of BCR/ABL fusion gene from a to g: (a) 0 fM (blank), (b) 1 fM, (c) 10 fM, (d) 100 fM, (e) 1 pM, (f) 10 pM, and (g) 100 pM. (B) Calibration curve of ECL intensity and logarithm of concentration of BCR/ABL fusion gene.

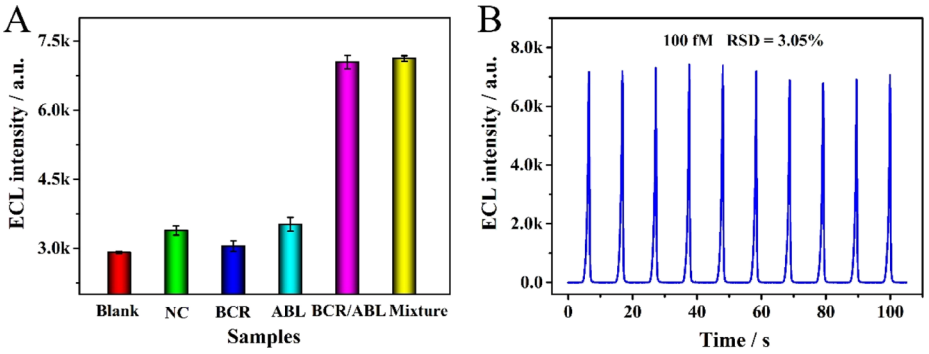

Figure 9. (A) Specificity of the ECL assay detection of BCR/ABL fusion gene against the interference substances: 1 pM NC, 1 pM normal BCR gene, 1 pM normal ABL gene, 100 fM BCR/ABL fusion gene, and mixture (1 pM NC, 1 pM normal BCR gene, 1 pM normal ABL gene, and 100 fM BCR/ABL fusion gene). (B) Stability of the ECL assay for the BCR/ABL fusion gene (100 fM) under continuous scanning for 10 cycles.

detected by this proposed ECL biosensor. It could be seen in Figure 8A that the ECL signal enhanced with the incremental concentration of BCR/ABL fusion gene from 1 fM to 100 pM. Moreover, the ECL signal showed an admirable linear relationship with the BCR/ABL fusion gene concentration (Figure 8B). The linear regression equation was $I = 1585.2 \lg c + 4173.4$ ($R^2 = 0.9983$), and the detection limit was calculated to be 0.18 fM (S/N = 3). Additionally, compared with other detection methods for BCR/ABL fusion gene determination (Table S2), it could be seen that the developed ECL biosensor possessed a broader linear range and a lower detection limit because of the well-regulated DNA walker signal amplification strategy.

Specificity and Stability of the ECL Biosensor. To investigate the specificity of the developed ECL biosensor, several interfering substances including normal BCR gene, normal ABL gene, and noncomplementary DNA (NC) were chosen. In Figure 9A, the ECL responses of nonspecific interfering substances were weak close to the blank despite the high concentrations (1 pM). Nevertheless, a significantly increased ECL signal was obtained at a lower concentration of target (100 fM), elucidating the high specificity of the ECL biosensing for the determination of the BCR/ABL fusion gene. Next, the ECL response of the mixture (1 pM normal BCR gene, 1 pM normal ABL gene, 1 pM NC and 100 fM BCR/ABL fusion gene) was approximate to that of single BCR/ABL fusion gene (100 fM). This indicated that these interfering substances hardly affected the response to the BCR/ABL fusion gene, manifesting the excellent specificity of the proposed ECL biosensing for the determination of BCR/ABL fusion gene.

The stability was another crucial parameter to appraise the reliability of a biosensor. To evaluate the stability in the long testing process, this biosensor was adequately executed through continuous scanning for 10 cycles. Relatively stable ECL intensity was observed under continuous scan with a relative standard deviation of 3.05% (Figure 9B), manifesting the favorable stability of this proposed biosensor.

CONCLUSIONS

In summary, well-regulated interfacial DNA tracks were constructed by fabricating long periodic linear DNA concatemers on the electrode surface, which remarkably promoted the walking efficiency of the bipedal DNA walker. Unlike the stochastic assembly of DNA tracks, these well-regulated tracks were favorable for DNA walking because of the well matching of equidistant foothold with bipedal walker and the relative weak steric effect. Utilizing the well-regulated track-based DNA walker as efficient signal amplification and Au@g-C_3N_4 NHs as excellent luminophores and nanocarriers, an ultrasensitive "off-on" ECL biosensor has been successfully fabricated for the BCR/ABL fusion gene detection. This ECL biosensing achieved rapid and sensitive detection of BCR/ABL fusion gene with the detection limit down to sub-femtomole level. Significantly, this well-regulated track-based DNA walker provided a valuable idea to construct a sensing interface with a high response rate as well as efficient signal amplification.

https://dx.doi.org/10.1021/acs.analchem.0c03893
Anal. Chem. 2020, 92, 15624−15631

■ ASSOCIATED CONTENT

Supporting Information

The Supporting Information is available free of charge at https://pubs.acs.org/doi/10.1021/acs.analchem.0c03893.

Reagents and materials, instruments, synthesis of g-C_3N_4 NSs, preparation of FA-BS, construction of type I and type II DNA walking machines, kinetics study of periodic linear dsDNA concatemers and diffusion dsDNA-based DNA walker amplification, comparison with previously reported methods, and preliminary analysis in serum samples (PDF)

■ AUTHOR INFORMATION

Corresponding Authors

Min Zhao − *Key Laboratory of Clinical Laboratory Diagnostics (Ministry of Education), College of Laboratory Medicine, Chongqing Medical University, Chongqing 400016, China*; Phone: +86-23-68485240; Email: zhaomin@cqmu.edu.cn

Wei Cheng − *Key Laboratory of Clinical Laboratory Diagnostics (Ministry of Education), College of Laboratory Medicine, Chongqing Medical University, Chongqing 400016, China; The Center for Clinical Molecular Medical Detection, The First Affiliated Hospital of Chongqing Medical University, Chongqing 400016, China;* orcid.org/0000-0002-1921-9761; Phone: +86-23-89011816; Email: chengwei@hospital.cqmu.edu.cn

Authors

Heye Lv − *Key Laboratory of Clinical Laboratory Diagnostics (Ministry of Education), College of Laboratory Medicine, Chongqing Medical University, Chongqing 400016, China*

Anyi Chen − *School of Public Health and Management, Chongqing Medical University, Chongqing 400016, China*

Wenqian Cheng − *Key Laboratory of Clinical Laboratory Diagnostics (Ministry of Education), College of Laboratory Medicine, Chongqing Medical University, Chongqing 400016, China*

Liangsheng Kong − *Key Laboratory of Clinical Laboratory Diagnostics (Ministry of Education), College of Laboratory Medicine, Chongqing Medical University, Chongqing 400016, China*

Shijia Ding − *Key Laboratory of Clinical Laboratory Diagnostics (Ministry of Education), College of Laboratory Medicine, Chongqing Medical University, Chongqing 400016, China;* orcid.org/0000-0002-9183-1656

Huangxian Ju − *State Key Laboratory of Analytical Chemistry for Life Science, School of Chemistry and Chemical Engineering, Nanjing University, Nanjing 210023, China;* orcid.org/0000-0002-6741-5302

Complete contact information is available at: https://pubs.acs.org/10.1021/acs.analchem.0c03893

Author Contributions

[⊥]H.L. and A.C. contributed equally to this work.

Notes

The authors declare no competing financial interest.

■ ACKNOWLEDGMENTS

This research was supported by the National Natural Science Foundation of China (no. 21804015 and no. 81873980), the Natural Science Foundation Project of CQ CSTC (no. cstc2018jcyjAX0206) and the National Science and Technology Major Project of the Ministry of Science and Technology of China (no. 2018ZX10732202).

■ REFERENCES

(1) von Delius, M.; Leigh, D. A. *Chem. Soc. Rev.* **2011**, *40*, 3656−3676.
(2) Valero, J.; Pal, N.; Dhakal, S.; Walter, N. G.; Famulok, M. *Nat. Nanotechnol.* **2018**, *13*, 496−503.
(3) Bazrafshan, A.; Meyer, T. A.; Su, H.; Brockman, J. M.; Blanchard, A. T.; Piranej, S.; Duan, Y.; Ke, Y.; Salaita, K. *Angew. Chem., Int. Ed.* **2020**, *59*, 9514−9521.
(4) Shin, J.-S.; Pierce, N. A. *J. Am. Chem. Soc.* **2004**, *126*, 10834−10835.
(5) Chen, A.; Zhuo, Y.; Chai, Y.; Yuan, R. *Chem. Commun.* **2019**, *55*, 13932−13935.
(6) Luo, J.-H.; Li, Q.; Chen, S.-H.; Yuan, R. *ACS Appl. Mater. Interfaces* **2019**, *11*, 27363−27370.
(7) Li, L.; Zhang, Y.; Yan, Z.; Chen, M.; Zhang, L.; Zhao, P.; Yu, J. *ACS Sens.* **2020**, *5*, 1482−1490.
(8) Peng, R.; Zheng, X.; Lyu, Y.; Xu, L.; Zhang, X.; Ke, G.; Liu, Q.; You, C.; Huan, S.; Tan, W. *J. Am. Chem. Soc.* **2018**, *140*, 9793−9796.
(9) Yao, D.; Bhadra, S.; Xiong, E.; Liang, H.; Ellington, A. D.; Jung, C. *ACS Nano* **2020**, *14*, 4007−4013.
(10) You, M.; Lyu, Y.; Han, D.; Qiu, L.; Liu, Q.; Chen, T.; Sam Wu, C.; Peng, L.; Zhang, L.; Bao, G.; Tan, W. *Nat. Nanotechnol.* **2017**, *12*, 453−459.
(11) Kopperger, E.; Pirzer, T.; Simmel, F. C. *Nano Lett.* **2015**, *15*, 2693−2699.
(12) Ge, J.; Zhao, Y.; Gao, X.; Li, H.; Jie, G. *Anal. Chem.* **2019**, *91*, 14117−14124.
(13) Zhao, M.; Bai, L.; Cheng, W.; Duan, X.; Wu, H.; Ding, S. *Biosens. Bioelectron.* **2019**, *127*, 126−134.
(14) Oishi, M.; Saito, K. *ACS Nano* **2020**, *14*, 3477−3489.
(15) Wang, Y.; Hu, N.; Liu, C.; Nie, C.; He, M.; Zhang, J.; Yu, Q.; Zhao, C.; Chen, T.; Chu, X. *Nanoscale* **2020**, *12*, 1673−1679.
(16) Zhang, J.; Lin, B.; Wu, L.; Huang, M.; Li, X.; Zhang, H.; Song, J.; Wang, W.; Zhao, G.; Song, Y.; Yang, C. *Angew. Chem., Int. Ed.* **2020**, *59*, 14115−14119.
(17) Yang, P.; Li, Y.; Mason, S. D.; Chen, F.; Chen, J.; Zhou, R.; Liu, J.; Hou, X.; Li, F. *Anal. Chem.* **2020**, *92*, 3220−3227.
(18) Liu, Z.; Lei, S.; Zou, L.; Li, G.; Xu, L.; Ye, B. *Biosens. Bioelectron* **2020**, *147*, 111759.
(19) Sherman, W. B.; Seeman, N. C. *Nano Lett.* **2004**, *4*, 1203−1207.
(20) Wang, D.; Vietz, C.; Schröder, T.; Acuna, G.; Lalkens, B.; Tinnefeld, P. *Nano Lett.* **2017**, *17*, 5368−5374.
(21) Yang, X.; Tang, Y.; Mason, S. D.; Chen, J.; Li, F. *ACS Nano* **2016**, *10*, 2324−2330.
(22) Jung, C.; Allen, P. B.; Ellington, A. D. *Nat. Nanotechnol.* **2016**, *11*, 157−163.
(23) Zhang, H.; Xu, X.; Jiang, W. *Chem. Sci.* **2020**, *11*, 7415−7423.
(24) Ge, J.; Li, C.; Zhao, Y.; Yu, X.; Jie, G. *Chem. Commun.* **2019**, *55*, 7350−7353.
(25) Chen, L.; Zeng, X.; Si, P.; Chen, Y.; Chi, Y.; Kim, D.-H.; Chen, G. *Anal. Chem.* **2014**, *86*, 4188−4195.
(26) Lv, Y.; Chen, S.; Shen, Y.; Ji, J.; Zhou, Q.; Liu, S.; Zhang, Y. *J. Am. Chem. Soc.* **2018**, *140*, 2801−2804.
(27) Liang, R.-P.; Yu, L.-D.; Tong, Y.-J.; Wen, S.-H.; Cao, S.-P.; Qiu, J.-D. *Chem. Commun.* **2018**, *54*, 14001−14004.
(28) Chen, A.; Liang, W.; Wang, H.; Zhuo, Y.; Chai, Y.; Yuan, R. *Anal. Chem.* **2020**, *92*, 1379−1385.